# An Efficient Diabetic Retinopathy Detection and Classification System Using LRKSA-CNN and KM-ANFIS

Rachna Kumari[1], Sanjeev Kumar[2] , Sunila Godara[3]
Research Scholar, Department of Computer Science & Engineering, Guru Jambheshwar University of Science & Technology, Hisar, India[1]
Professor, Department of Computer Science & Engineering, Guru Jambheshwar University of Science & Technology, Hisar, India[2, 3]

***Abstract*—If Diabetic Retinopathy (DR) is not diagnosed in the early stages, it leads to impaired vision and often causes blindness. So, diagnosis of DR is essential. For detecting DR and its diverse stages, various approaches were developed. However, they are limited in considering microstructural changes of visual pathways associated with the visual impairment of DR. Thus, this work proposes an effective Linearly Regressed Kernel and Scaled Activation-based Convolution Neural Network (LRKSA-CNN) to diagnose DR utilizing multimodal images. Primarily, the input Optical Coherence Tomography (OCT) image is preprocessed for contrast enhancement utilizing Contrast-Limited Adaptive Histogram Equalization (CLAHE) and resolution enhancement utilizing the Gaussian Mixture Model (GMM). Likewise, the Magnetic Resonance Imaging (MRI) image's contrast is also improved, and edge sharpening is performed utilizing Unsharp Mask Filter (USF). Then, preprocessed images are segmented utilizing the Intervening Contour Similarity Weights-based Watershed Segmentation (ICSW-WS) algorithm. Significant features are extracted from the segmented regions. Next, important features are chosen utilizing the Min-max normalization-based Green Anaconda Optimization (MM-GAO) algorithm. By utilizing the LRKSA-CNN technique, the selected features were classified into DR and Non-Diabetic Retinopathy (NDR). Hence, utilizing the Krusinka Membership-based Adaptive Neuro Fuzzy Interference System (KM-ANFIS), various stages of DR were classified based on the presence of intermediate features. Lastly, the proposed system achieves superior outcomes than the baseline systems.**

***Keywords*—Intervening contour similarity weights based watershed segmentation (ICSW-WS); min-max normalization based green anaconda optimization (MM-GAO); krusinka membership based adaptive neuro fuzzy interference system (KM-ANFIS); linearly regressed kernel and scaled activation based convolution neural network (LRKSA-CNN); and deep learning**

## I. Introduction

The well-known reason for visual deficiency is DR, which is also known as diabetic eye disease. DR has turned into a global pandemic with 365 million individuals expected to be impacted by 2025 [1]. People who have diabetes for a long duration are more likely to develop DR, and it impressively causes vision loss by the gradual destruction of the retina's blood vessels over a while [2]. Lesions like Neovascularization (NV), exudates, hemorrhages, and microaneurysms may develop in DR patients. For proper intervention, these lesions need to be detected early. Thus, to manage DR and prevent progression, early detection and treatment are the most efficient ways [3] [4].

Various tasks associated with automatic DR diagnosis have been performed in the past decades. The automatic classification of DR from retinal images is increasingly studied owing to the huge number of diabetic patients and the need for more accurate and automatic diagnosis [5]. Artificial Intelligence (AI) can help in solving this problem. For analyzing raw medical images from beginning to end and predicting a goal result, Deep Learning (DL), particularly, Deep Convolutional Neural Networks (DCNN) and Deep Neural Networks (DNNs) can be utilized [6] [7].These systems have been trained on tens of thousands of medical images and demonstrated screening performance similar to that of retinal specialists [8]. Various screening tools are available to receive those kinds of medical images, such as the visual acuity test, OCT, colour fundus camera, eye angiography, and so on [9] [10]. The conventional screening of fundus images to diagnose DR lesions takes time, thus delaying therapy and minimizing the chance of success [11]. But, severe bleeding symptoms cover NV outside the macula in fundus photography, which leads to misdiagnosis [12]. However, evaluating the intensity of retinopathy in people with diabetes is mostly dependent on human assessment of retinal fundus pictures, which is complicated to perform [13] [14]. These problems can be alleviated via the use of OCT, which together provide micrometer-scale resolution structural, 3-dimensional (3D), depth-resolved, and vascular images of the retina [15]. But, recent studies showed that visual deficiency for DR is also associated with the pathophysiological changes of different parts of the visual pathway. To maintain visual function, the evaluation of the progressive visual pathway along with the visual field is considered to be a vital process.

### A. Problem Statement

Most of the prevailing models developed for DR diagnosis were limited in solving the following challenges:

- Limited research was performed for exposing the invisible pathophysiological mechanism i.e.,

pathophysiological changes and related damages to the different retinal layers along with the cerebral visual pathway to diagnose diabetic retinopathy.

- Improper segmentation of small regions was caused by the loss of apparent activity in tiny objects or else regions due to the imaging systems' limited resolution that is, blurring of intensities near their edges.
- Owing to the poor image resolutions and the inability of such images to exhibit more pixel information, the segmentation techniques were ineffective on OCT images and ignored detailed information.
- Prevailing techniques utilized limited features and the model often predicted near the same value due to the exclusion of some key features, which influenced the outcome of the prediction system.
- Prevailing techniques utilized limited features, and the exclusion of some key features caused the model to often predict near the same value, which might influence the outcome of the prediction system.

Thus, for solving the aforementioned problems, this paper proposes an effective LRKSA-CNN-based DL technique for DR diagnosis. The proposed system includes the subsequent contributions:

- A multimodal imaging strategy is used to explore microstructural changes in the visual pathway and invisible pathologies inside the retina structure.
- To recover blurred intensities of edges, remove imperfections in the images, and make edges easier to the visible edge, sharpening is performed to avoid improper segmentation of small regions.
- The finer details of images were accurately revealed via the resolution enhancement of OCT images utilizing the PIR technique to improve the segmentation accuracy.
- Along with the intermediate features, the global and local features were also extracted, which enhances the model efficiency to better explore the progression of eye disease.

This paper's remaining portion is aligned as: Section II reviews the associated works, Section III describes the proposed technique, Section IV propounds the experimental outcomes and discussion, and Section V concludes the paper.

## II. Related Literature Survey

M. Sakthisreedevi *et al.* [16] detected DR by identifying its features in OCT images. Utilizing the graph-cut technique, 7 retinal layers were segmented from the OCT images. Next, the features of retinal layers were extracted for differentiating normal and DR subjects. Experimental outcomes showed that for diagnosing DR, the extracted features were effective. But, the system was limited in specifying the classification process. Mahmoud Elgafi *et al.* [17] propounded a three-step model for DR detection using OCT images. The retinal layers were segmented and the 3D features were extracted from every single layer. Utilizing Backpropagation Neural Networks (BPNN), the features were classified. Experimental outcomes displayed the recommended technique's potential for DR detection using OCT images. But, the system accuracy was poor owing to the usage of limited data. Brahami Menaouer *et al.* [18] established a hybrid DL technique for DR detection. DCNN and Visual Geometric Group (VGG) network models-centric classification were followed in this model. The classification as per the visual risk was related to the retinal ischemia's severity. According to the experimental outcomes, the hybrid technique diagnosed DR accurately with more speed. The model's major limitation was the increased training time to train its parameters. Sambit S. Mondal *et al.* [19] presented an automated ensemble DL system for DR detection. The images were pre-processed and augmented utilizing a General Adversarial Network (GAN).For DR detection, the modified DenseNet101 and ResNet DL systems were the ensemble. The comparison exhibited that for DR classification, this technique had high accuracy. But, the system accuracy was low for five classes rather than two classes. M. Murugappan *et al.* [20] implemented the Few Shot Learning (FSL) classification networks to grade and detect DR centered on the attention mechanism. The model utilized an episodic learning strategy and attention mechanism for the few-shot classification task. As per the analysis of performance metrics, the model effectively detected DR. However, to prove the efficiency of the developed system, the comparison made in the paper was limited. Muhammad Mohsin Butt *et al.* [21] recommended a hybrid technique for DR detection as well as classification in fundus images. Utilizing transfer learning-based CNN, the features were extracted. The features were merged into a hybrid feature vector and utilized for the DR classification. Experimental outcomes revealed that significant performance improvement was provided by the model. But, the supremacy of model performance was degraded by the poor quality of input images. Abdüssamed Erciyas & NecaattinBarışçı [22] propounded a DL-centric framework for DR lesions' detection and classification. The DR lesions were detected from the DR data and marked utilizing Regional CNN (FRCNN).By utilizing the transfer learning and attention mechanism, the images from FRCNN were categorized. The result comparison showed that the developed system acquired more successful outcomes. Still, the system utilized larger computational resources. Mohamed Elsharkawy *et al.* [23] established an OCT-centric diagnosis technique for detecting DR. By utilizing prior shape knowledge, the model segmented the retinal layers. For global subject diagnosis, the classification was performed utilizing an Artificial Neural Network (ANN). The comparison outcomes indicated the ability of the system for diagnosing DR. However, the model attained poor classification accuracy owing to the limited number of features. Wejdan L. Alyoubi *et al.* [24] executed DR images' classification under various stages and localization of affected lesions. Two DL models, namely CNN-512 for classification and the YOLOv3 system for localizing DR lesions were utilized. The DR images were classified into five DR stages. The YOLOv3 model cannot detect smaller DR lesions owing to its anchor box design even though the acquired accuracy exceeded baseline outcomes. Mohammed Ghazal *et al.* [25]

concentrated on detecting Non-Proliferative DR (NPDR) utilizing CNN. Initially, the retina patches were extracted. Transfer learning centered on 2 pre-trained CNNs was utilized, where one was independently fed by nasal retina patches and the other one by temporal retina patches. The outcomes showed that the system attained a promising accuracy. But, the improper alignment of patches led to lower accuracy of the model. S. K. Sahu *et al.* [26] implemented different AI-based transfer learning models for diabetic retinopathy at early stages. The accuracy transfer learning models ranges from 74% to 81. S. Goswami [27] proposed an iterative attentional feature fusion (iAFF) method for DR detection. Model used InceptionV3 and Xception feature extraction. IDRiD data set was used for training and testing purpose. N. Z. Abidin and A. Ritahani Ismail [28] propose a federated deep learning model eliminate the need of pooling data in a single location. This model allowed deep learning algorithms to train from diverse sets of data from different sources. O. F. Gurcan *et al.* [29] proposed a metaheuristic algorithm based on deep learning for DR detection. In Model InceptionV3 was used to extract feature. The transfer learning method is applied in the extraction process. Particle Swarm optimization and Artificial Bee Colony were used for feature selection. Which were further classified eXtreme Gradient Boosting (XGBoost). M. Jahiruzzaman [30] proposed a k-means color compression technique to detect hemorrhages and exudates in color fumdus images. The different region of fundus images were segmented out and classified using fuzzy inference system. M. Ghazal [31] proposed a computer aided diagnostic (CAD) system using CNNs for non-proliferative DR (NPDR) detection at early stage. A two pre-trained CNNs, one is independent fed of nasal retina patches and the other is by temporal retina patches was used to optimize the performance of model which was accuracy of 94%. H. Mustafa *et al.* [32] proposed a multi-stream ensemble deep network to categorize DR severity at different stages. Model utilizes benefits of the deep networks and principal component analysis (PCA) to train inter-class and intra-class variations from image features. Pre-trained deep learning architecture DenseNet-121 was used to extract main feature and Ensemble machine learning classifiers PCA was applied to classify images. Further AdaBoost and random forest algorithms were applied to improve classification accuracy. K. Aurangzeb *et al.* [33] implemented a ColonSegNet model for retinal vessel segmentation. This method efficiently locate vessels and applied data augmentation to resolve fewer graded images issues using intelligent evolution algorithms optimal values for the contrast enhancement were identified. DRIVE, CHASE_DB, and STARE datasets were used for training and testing purpose. M. Nur-A-Alam [34] proposed an automatic and intelligent system to classify DR images. First retinal images were pre-processed, then histograms of oriented gradient (HOG), Shearlet transform, and Region-Based Convolutional Neural Network (RCNN) were used to extract discriminating features and merged features as one fused feature vector. By using the fused features, a faster RCNN classifier was used to DR severe stages. R. Pires et al. [35] presented the bag-of-visual-words (BoVW) based algorithm for lesion detection in retinal images. The input of the metaclassifier work as output 9BoVW) of several lesion detectors. This algorithm create a high-level feature representation for the retinal images to lesion detection. M. T. Islam *et al.* [36] proposed a multi-stage convolutional neural network (CNN)-based model DiaNet to DR. study of this paper revealed that fundus images restrain sufficient information to differentiate the Qatari diabetes cohort from the control group. D. Maji [37] proposed a novel deep learning approach for retinal blood vessel and DR. The EfficientNet model was used with pre-trained weights facilitating transfer learning and optimize convergence speed. X. Wang *et al.* [38] proposed a supervised deep learning framework for macula-related disease classification with uncertainty estimation. In their model a convolutional neural network based instance-level classifier was refined by through uncertainty-driven deep learning method. Second, a recurrent neural network extract features and generated bag-level. M. M. Farag *et al.* [39] proposed a noval deep-learning-based method for DR detection using a single Color Fundus photograph. Authors employed DenseNet169's encoder to assemble a visual embedding. Then, Convolutional Block Attention Module (CBAM) was utilized to reinforce its discriminative power. At last, the model was trained on (APTOS) dataset using cross-entropy loss. T. Liu *et al.* [40] proposed a novel deep symmetric convolutional neural network to detect the microaneurysms (MAs) and hard exudates (HEs) of DR. Furthermore, different convolution pooling structures were practiced to obtain feature filtering in feature extraction phase. They concluded that microaneurysms detection was improved by using ave-pooling layer. G. T. Reddy *et al.* [41] implemented Linear Discriminant Analysis (LDA) and Principal Component Analysis (PCA) dimensionality reduction techniques, on Random Forest Classifier, Decision Tree Induction, Naive Bayes Classifier and Support Vector Machine (SVM), using Cardiotocography (CTG) dataset. From their paper it is concluded that performance of the classifiers, Random Forest, Decision Tree is not much affected by PCA and LDA. E. O. Rodrigues *et al.* [42] proposed a new ELEMENT (vEsseL sEgmentation using Machine lEarning and coNnecTivity) framework for vessel segmentation. Features were extracted based on vessel connectivity and grey level properties. This model speeds up the segmentation throughput and minimize. S. Wang *et al.* [43] proposed an integrated machine learning approach for microaneurysms detection. In this method first Candidate objects were located through a dark object filtering process. Then correlation coefficient between each processed profile and MA profile was determined. Furthermore, K-nearest neighbor classifier was applied to extract set of statistical features. K. Shankar *et al.* [44] proposed an automated Hyperparameter Tuning Inception-v4 (HPTI-v4) model for DR detection. At the preprocessing stage, contrast limited adaptive histogram equalization (CLAHE) was used to improve the contrast level of images. Furthermore, the HPTI-v4 model was employed to extract the essential features from the segmented image and then multilayer perceptron (MLP) was used for classification. B. Yang *et al.* [45] implemented a global channel attention mechanism (GCA) framework to detect DR at early stages. In this module, a one-dimensional convolution kernel size algorithm was used and GCA-EfficientNet (GENet) was employed to classify images. Experimental outcomes

conclude that GENet are more effective to extract lesion features and classify DR stages. I. Usman and K. A. Almejalli [46] implemented a new machine learning technique based on Genetic Programming for MAs detection in retinal images. The optimal expression was evolved generation by generation using the binary fitness scores and a stepwise enhancement process. The best expression obtained was then used as a classifier MA. B. Abdillah *et al.* [47] implemented texture feature model based on Local Binary Pattern for DR detection. k-Nearest Neighbor (k-NN) and Support Vector Machines (SVM) was used for classification of images. M. J. J. P. van Grinsven et al. [48] proposed a CNN based method for detection of hemorrhages in retinal images. Based on current status of CNN, Training samples were heuristically misclassified negative samples and weights are assigned in the next CNN training iteration. A. Krestanova *et al.* [49] reviewed all segmentation techniques for retinal blood vessel extraction. Their review included analysis of segmentation techniques based on degree of curvature of retinal blood vessels and objectification parameters. They reviewed all calculations and metrics to obtain the degree of tortuosity of retinal blood vessels. K. Wisaeng and W. Sa-Ngiamvibool [50] proposed a mathematical morphology algorithm to localize OD. Firstly, a coarse segmentation method was utilized to obtain exudates and non-exudates candidates. Finally, mathematical morphology algorithm was applied to classify exudates pixels. X. Li *et al.* [51] proposed a self-supervised learning model for DR detection. They used a rotation-oriented collaborative method to extract rotation-related and rotation-invariant features. Model was evaluated on two public datasets. G. Gupta [52] proposed a supervised learning framework based on micro-pattern of local variations using texture based analysis to localize patches colored fundus images. Rule-based criteria was used to determine the presence or absence of PDR. R. Kommaraju and M. S. Anbarasi [53] developed a machine learning framework to detect DR at early stages of color fundus images. Their model employed a swin transformer to detect the type of DR and Contrast Limited Adaptive Histogram Equalization (CLAHE) technique was used for image enhancement and flip for data augmentation. R. Gambhir [54] proposed a Shufflenetv2 method to detect DR at severity levels. Smooth L2 loss had been used to improve performance of model.

## III. Proposed Diabetic Retinopathy Detection System

The proposed model is a type for analyzing both the invisible pathologies on different retinal layers and pathophysiological changes on various parts of the visual pathway. For attaining this, the proposed LRKSA-CNN model is trained on multimodal medical images like OCT and fMRI. Fig. 1 displays the proposed system's detailed workflow.

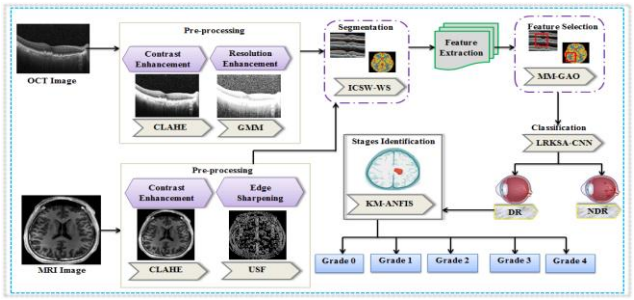


Fig. 1. Block diagram of the proposed methodology.

### A. Preprocessing

The proposed technique's initial phase is preprocessing in which input OCT and MRI images are preprocessed for contrast enhancement. Since these images were obtained under various lighting conditions, they have lower contrast and require to be preprocessed before the execution model training. Thus, by utilizing the CLAHE technique, the input images' contrast was improved. Let $\left(R = \left\{R_{O(n)}, R_{M(n)}\right\}_{n=1}^{N}\right)$ be the set of input images, including two types of images, namely OCT $\left(R_{O(n)}\right)$ and MRI $\left(R_{M(n)}\right)$. These images are divided into smaller blocks $\left(R_m\right)$ by CLAHE, which computes the histogram $\left(\wp i(R_m) = \frac{\aleph_j}{\aleph_{avg}}\right)$ individually for each block. In the computation of the histogram, the average number of pixels per region is calculated as,

$$\aleph_{avg} = \frac{\aleph_h \times \aleph_v}{\aleph_{gr}}, \qquad \aleph \in R \tag{1}$$

Here, $\aleph_{avg}$ is the average number of pixels, $\aleph_{gr}$ is the number of grey levels, and $\aleph_h$ and $\aleph_v$ are the number of pixels in the horizontal and vertical dimensions. Subsequently, the clip limit to clip the histogram $\left(\wp i(R_m)\right)$ is defined and employed for the histogram as,

$$\aleph_\ell = \aleph_{avg} \times \aleph_{n\ell} \tag{2}$$

$$\wp i(R_m) = \begin{cases} \aleph_\ell & if\left(\aleph_j \geq \aleph_\ell\right) \\ \aleph_j & Otherwise \end{cases} \tag{3}$$

Here, $\aleph_j$ specifies the pixels with intensity $(j)$, $\aleph_{n\ell}$ indicates the normalized level of contrast enhancement, and $\aleph_\ell$ depicts the clip limit. Next, the clipped pixel values are computed for evenly redistributing the clipped pixel values below the histogram.

$$\aleph_p = (\aleph_h \times \aleph_v) - \sum_{i=1 to K-1} \wp i(R_m) \quad (4)$$

Here, $\aleph_p$ depicts the number of clipped pixels, and $K$ symbolizes the total number of grey levels. Next, the clipped histogram is normalized as,

$$\wp i(R_m) = \begin{cases} \aleph_\ell & if\left(\aleph_j + \frac{\aleph_p}{K} \geq \aleph_\ell\right) \\ \aleph_j + \frac{\aleph_p}{K} & Otherwise \end{cases} \quad (5)$$

Till all the pixels are redistributed, these steps are continued, and the cumulative histogram of every single region is calculated for grey-level mapping. Lastly, the histogram of each region is matched for computing the weighted sum of $(m_{1,2,3,4})$ neighboring regions, and the enhanced output is acquired by the interpolation of neighboring regions. The output image is acquired as,

$$R_{ce} = (1-h)(1-v) \times R_{m1} + h \times R_{m2} + v \times (1-h) \times R_{m3} + h \times R_{m4} \quad (6)$$

Here, $\left(R_{ce} = \{R_{eO(n)}, R_{eM(n)}\}_{n=1}^{N}\right)$ are the output-enhanced images, and $(h)$ and $(v)$ are the horizontal and vertical distances corresponding to the region.

From the preprocessed images, OCT images' spatial resolution is enhanced, and edge sharping for MRI images is performed.

*1) Resolution enhancement of OCT*: Here, the quality of $(R_{eO(n)})$ as OCT images' lower spatial resolution affects the segmentation outcome. Enhancing the resolution of OCT images gives vital information held in each pixel suitable for decision-making at the regional level. Thus, the patch-centric resolution enhancement utilizing GMM is given below:

The resolution enhancement technique executes the task of reconstructing the enhanced image $(R_{seO(n)})$ of *the input image* $(R_{eO(n)})$ centered on the low-resolution observation $(R_{lrO(n)})$ utilizing GMM. The enhanced image $(R_{seO(n)})$ is reconstructed by solving the following objective function as,

$$\arg\min_{R_{seO(n)}} \left\| \partial R_{eO(n)} - R_{lrO(n)} \right\|^2 - \sum_{i \in R} \log \hat{\lambda}\left(R_{eO(n)}, i\right) \quad (7)$$

Here, $\partial$ signifies the unknown operator for generating low-resolution observation $(R_{lrO(n)})$, $R_{lrO(n)}$ indicates the observed low-resolution image, $\hat{\lambda}$ symbolizes the probability density function, and $(R_{eO(n)}, i)$ are the patches in the input image.

To reconstruct the high-resolution image, the reference images $\{R'_{lrO(n)}, R'_{hrO(n)}\}$ are considered. From them, the low-resolution $\{R'_{lrO(n)}, i\}$ and high-resolution $\{R'_{hrO(n)}, i\}$ patches are extracted and concatenated $R' = \begin{pmatrix} R'_{lrO(n)} \\ R'_{hrO(n)} \end{pmatrix}$ for obtaining the parameters of GMM $(\alpha, \beta, \gamma, \lambda)$. The $\{R_{hrO(n)}, i\}$ from $(R_{eO(n)})$ is computed by choosing the best component of GMM as,

$$\chi = \arg\max_{\chi} \alpha \, p\left(R_{lrO(n)} \mid \alpha, \beta, \gamma, \lambda\right) \quad (8)$$

Here, the likelihood $(p)$ of $\{R_{lrO(n)}, i\}$ to the $\chi$ component is maximal. Using the parameters, the high-resolution patch $\{R_{hrO(n)}, i\}$ is computed as,

$$R_{hrO(n)} = \alpha_{hr,\chi} + \sum_{hr,lr,\chi} \sum\nolimits_{lr,\chi}^{-1} \left(R_{lrO(n)} - \alpha_{lr,\chi}\right) \quad (9)$$

Here, the high-resolution patches $(R_{hrO(n)})$ are centered on the parameters of the generalized Gaussian mixture $\alpha_{hr,\chi}$. From all the estimated high-resolution patches, the high-resolution image $(R_{seO(n)})$ is reconstructed and utilized as input for the segmentation. This phase ignores the MRI images since they have better contrast resolution properties to extract images' finer details.

2) *Edge sharpening*: Here, the preprocessed MRI image $(R_{eM(n)})$ is utilized to recover edges that have been blurred owing to the partial volume effect. By doing so, the ideal boundary between two structures is restored for quantitatively distinguishingvarious types of tissues in the segmentation process. When performing edge sharpening for the OCT images, the noise in the image is also enhanced; thus, it becomes less natural and the level of information in flat and smooth areas is lost. Thus, the OCT images were not considered here. The USF is utilized for edge sharpening.

The main purpose of a USF is to subtract an unsharp mask from the input image. For this, the unsharp mask, that is, the original image's even more blurred version is yielded by spatially filtering the input image utilizing a Gaussian low-pass filter. The Gaussian function is derived as,

$$\eta(a,b) = \frac{1}{\varpi\sqrt{2\pi}} \exp\left(\frac{-a^2 - b^2}{2\varpi^2}\right) \quad (10)$$

Here, $\eta(a,b)$ indicates the Gaussian function, $\varpi$ signifies the standard deviation value, and $\pi$ specifies the weight mixing coefficient. The original image's Gaussian blurred version is acquired as,

$$R_{mM(n)} = \eta(a,b) * R_{eM(n)} \quad (11)$$

Next, the unsharp mask $\left(R_{mM(n)}\right)$ acquired is subtracted from the input image for getting edges as,

$$R_{sM}(n) = \frac{e}{2e-1} R_{mM}(a,b) - \frac{1-e}{2e-1} R_{eM}(n) \quad (12)$$

Here, $R_{sM}(n)$ symbolizes the output image, $e$ is the constant to control the weightings of images, and $R_{mM}(a,b)$ indicates the brightness values of pixels at coordinates $(a,b)$ in the unsharpmask $R_{mM}$ .

### B. Segmentation

After the success of resolution enhancement and edge sharpening, the resultant images $\left(R_{enh} = \{R_{seO(n)}, R_{sM(n)}\}\right)$ are subjected to the ICSW-WS algorithm for segmentation. The Watershed Segmentation (WS) algorithm is utilized as it can handle images with a considerable amount of irregular shapes and noise. But, the WS has the over-segmentation issue while a large number of small regions arise. For solving this problem, the conventional watershed algorithm calculates the intervening contour similarity weights. Hence, the segmentation is described below: Primarily, the input images are converted into greyscale, and local minima in the image are found. For this, by computing the intervening similarity weights, the watershed line between the two regions is created. The over-segmentation issue occurs as the segmentation process contains the segmentation of smaller regions. For solving this, the intervening similarity measure is computed as,

$$R_{wr} = \sqrt{\sum_{i=1ton} \left\| R_{enh(r1,i)} - R_{ref(r1,j)} \right\|_2} \quad (13)$$

Here, $R_{wr}$ is the output image with weighted regions, and $R_{enh(r1,i)}, R_{ref(r1,j)}$ are the regions with different pixel values $(i, j)$ in the reference image and input image. The similarity measure has the benefit of informing the intervention of another region, thus forming the outer contour of the region. Like this, the relation between the data samples was measured; for providing different regions of the image, the border information is jointly integrated.

After marking the regions, the algorithm floods the image with various colors and the color spreads for creating catchment basins by reaching the region boundary. The basins are formed utilizing the watershed function as,

$$R_{seg} = \varphi_{wsf}(d, R_{wt}) \quad (14)$$

Here, $d$ signifies the point in the domain of the watershed function, $R_{wt}$ indicates the regions assigned with the intervening weights, and $\varphi_{wsf}$ specifies the watershed function.

In the proposed system, segmentation is performed in two different ways. The significant retinal layers are segmented from the OCT images for evaluating invisible changes in the retina. For segmenting the visual networks, namely posterior cingulate, calcarine, inferior parietal lobule, precuneus, lingual gyrus, cerebellum, and cuneus, the MRI images were utilized for analyzing the pathophysiological changes in the visual pathway. Thus, the segmented images are indicated as $\left(R_{seg} = \{R_{segO(n)}, R_{segM(n)}\}\right)$.

### C. Feature Extraction

After segmentation, the significant features are extracted from $\left(R_{seg} = \{R_{segO(n)}, R_{segM(n)}\}\right)$ . The proposed system extracted regional homogeneity, degree centrality, and Amplitude of Low-Frequency Fluctuations (ALFF) features from the visual network regions $\left(R_{segO(n)}\right)$, and reflectivity, curvature, volume, and thickness features from the segmented retinal layers $\left(R_{segM(n)}\right)$. Moreover, the global and local features to find interest points, contour, shape, texture, and visual information useful for class discrimination are extracted. Thus, the extracted features are given as,

$$\nabla_{fea(n)\in R_{seg}} = \{\nabla_{fea\in R_{segO(n)}}, \nabla_{fea\in R_{segM(n)}}, \nabla_{lfea\in R_{seg}}, \nabla_{gfea\in R_{seg}}\} \quad (15)$$

Here, the set of total features is signified as $\nabla_{fea(n)\in R_{seg}}$ , the features extracted from the retinal layers and visual network areas are indicated as $\nabla_{fea\in R_{segO(n)}}, \nabla_{fea\in R_{segM(n)}}$ , and the global and local features are symbolized as $\nabla_{lfea\in R_{seg}}, \nabla_{gfea\in R_{seg}}$ .

### D. Feature Selection

Here, the subset of the most relevant features is chosen from $\left(\nabla_{fea(n)\in R_{seg}}\right)$ for enhancing the system's performance. The MM-GAO algorithm is used for feature selection. The Green Anaconda Optimization algorithm is utilized for its ability to tackle a wider range of prey. However, the probability function of pheromone concentration in this algorithm only concentrates on maximum values, which leads to high risk of competition for captured food as it can't handle the minimum objective function. Thus, for solving this problem, the min-max normalization approach is

utilized in the prevailing green anaconda optimization algorithm for evaluating the probability of pheromone concentration.

In the MM-GAO algorithm, the positions of its population members are considered as the number of features extracted $\left(\nabla_{fea(n)\in R_{seg}}\right)$ from which the optimal solutions are chosen. The position of each green anaconda is randomly generated, and the objective function of problem space is calculated. It can be exposed as,

$$\nabla_{fea(n)} = \begin{bmatrix} \nabla_{fea(1,1)} & \cdots & \nabla_{fea(1,1)} \\ \vdots & \cdots & \vdots \\ \nabla_{fea(n,1)} & \cdots & \nabla_{fea(n,m)} \end{bmatrix} \quad (16)$$

$$\vartheta\left(\nabla_{fea(n)}\right) = \arg\min_{\nabla_{sf(n)}} \left|\xi_{tar(DR,NDR)} - \xi_{act(DR,NDR)}\right| \quad (17)$$

Here, $m$ indicates the number of decision variables, $\vartheta(\bullet)$ signifies the objective function, and $|\bullet|$ depicts the distance between the actual output $\left(\xi_{act(DR,NDR)}\right)$ and the target $\left(\xi_{tar(DR,NDR)}\right)$ of the classifier output.

In the search process, the best value as per the objective function is chosen via two phases, namely exploration and exploitation.

Exploration: Here, the mating season of male and female anacondas is done. For updating the position of the green anaconda, the species strategy of the male is used. Utilizing this strategy, the male anaconda senses the pheromones, indicating the presence of the female anaconda, and moves towards it.

The set of female species is determined as,

$$\nabla_{FL(n)} = \left\{\nabla_{fea(k_n)} : \vartheta\left(\nabla_{fea(k_n)}\right)\right\}, \quad k_n \neq n \quad (18)$$

Here, $\nabla_{FL(n)}$ signifies the set of female species for each green anaconda in the first row of the population matrix $k_n$. Next, the probability of pheromone concentration for each population member utilizing the min-max approach is computed as,

$$\Phi_{(n,q)} = \sum_{l} \frac{\vartheta_l\left(\nabla_{fea(k_n)}\right) - \vartheta_{\min}\left(\nabla_{fea(k_n)}\right)}{\vartheta_{\max}\left(\nabla_{fea(k_n)}\right) - \vartheta_{\min}\left(\nabla_{fea(k_n)}\right)} \quad (19)$$

Here, $\Phi_{(n,q)}$ depicts the probability pheromone concentration of the $q^{th}$ female for the $n^{th}$ green anaconda, $\vartheta_l\left(\nabla_{fea(k_n)}\right)$ signifies the set of objective values of the candidate female, and $\vartheta_{\min}\left(\nabla_{fea(k_n)}\right)$, $\vartheta_{\max}\left(\nabla_{fea(k_n)}\right)$ are the minimum and maximum values.

The min-max approach assures the green anaconda's maxmin value to limit its search between minimum and maximum values, thus evaluating the minimum or maximum probability value that limits them in capturing food. Thus, the min-max approach finds the optimal move for the search agent via the complete assessment of search spaces and accelerates the decision-making process for quick convergence.

During exploration, the green anaconda randomly chooses a female species and moves towards it. Therefore, the green anaconda's position is updated as,

$$\nabla_{sFL(n)} = \nabla_{FL} : \Phi_{FL(n-1,q)} < \nabla_{sFL(n)} < \Phi_{FL(n,q)} \quad (20)$$

$$\Phi_{FL(n,q)} = \Phi_{(n,q)} + \Phi_{FL(n-1,q)} \quad (21)$$

$$^{d}\nabla_{fea(n,i)} = \nabla_{fea(n,i-1)} + \nabla_{fea(n,i-1)}\left(\nabla_{sFL(n,i-1)} - \tau.\nabla_{fea(n,i-1)}\right) \quad (22)$$

Here, $\nabla_{sFL(n)}$ signifies the selected female species, $\Phi_{FL(n,q)}$ depicts the cumulative probability function, $\nabla_{sFL(n)}$ symbolizes the random number, $^{d}\nabla_{fea(n,i)}$ is the newly updated position of the green anaconda in $d$ dimensional search space, and $\nabla_{fea(n,i-1)}$ specifies the position updated in the prior iteration. Next, the objective function is assessed for updating the best solution.

Exploitation: Here, the hunting strategy of the green anaconda is followed in which it waits for the prey underwater, and when the prey passes, the anaconda surrounds and attacks the prey. Here, to obtain possible better solutions in local search, the position of group members is updated. The position is updated as,

$$\nabla_{fea(n,i)} = \nabla_{fea(n,i-1)} + (1-\tau)\frac{U-L}{i} \quad (23)$$

Here, $U, V$ are the $d$-th search space's upper and lower bounds, and $i$ indicates the number of iterations. Till the algorithm's last iteration, the updating process continues. The feature selection strategy utilizing the MM-GAO algorithm is displayed in Algorithm 1.

**Algorithm 1:** Feature Selection using MM-GAO

**Input:** Extracted feature $\left(\nabla_{fea(n)\in R_{seg}}\right)$

**Output:** Selected features $\nabla_{sf(n)}$

**Begin**

**Initialize** input data $\left(\nabla_{fea(n)\in R_{seg}}\right)$, parameters $\tau$ , $\Phi$ and $\vartheta$ , number of iterations $i$

**Compute** fitness of each individual $(\vartheta)$

**Select** best solution

**While** $(i < i_{\max})$

**Identify** female species $\left(\nabla_{FL(n)}\right)$ //Exploration

**Compute** probability of pheromone concentration $\left(\Phi_{(n,q)}\right)$

**Determine** selected females $\nabla_{sFL(n)}$

**Update** new position ${}^{d}\nabla_{fea(n,i)}$

**For** each updated position **do**

**If** $\vartheta\left(\nabla_{fea(n,i)}\right) < \vartheta\left(\nabla_{fea(n,i-1)}\right)$

**Update** $\nabla_{fea(n,i)}$ as best-fit position

**Else**

**Keep** previous solution $\nabla_{fea(n,i-1)}$

**End if**

**Ed for**

**Update** new position using hunting strategy $\nabla_{fea(n,i)}$ //exploitation

**Update** best solutions

**Set** $i = i + 1$

**End while**

**Return** selected features $\nabla_{sf(n)}$

**End**

The best solutions were filtered in each iteration by using the exploration and exploitation phases after updating the position of all green anacondas. In this way, the optimal features are selected by utilizing the MM-GAO algorithm, and the selected features are given as,

$$\nabla_{sf(n)} = \begin{cases} \nabla_{fea(n,i)} & \vartheta\left(\nabla_{fea(n,i)}\right) < \vartheta\left(\nabla_{fea(n,i-1)}\right) \\ \nabla_{fea(n,i-1)} & Otherwise \end{cases} \quad (24)$$

Here, the total number of selected features is signified as $\nabla_{sf(n)}$.

*E. Classification*

For classification using anLRKSA-CNN, the selected features from the above phase $\left(\nabla_{sf(n)}\right)$ are utilized. CNN is selected as it is really efficient for image classification since the dimensionality reduction concept suits the huge number of parameters in an image. But, fixed kernel size utilization causes the loss of significant information hidden in unexplored regions, and the learning process is slowed down by the activation function utilized in the convolution layer owing to the biased shift effect. For overcoming this, the traditional CNN includes Linear Regression-based modeling of kernel size and Scaled Lineartanh (SLT) activation function for the convolution layer. Fig. 2 displays LRKSA-CNN's architecture.

Initially, the extracted features were inputted to the convolution layer. The convolution layer seeks to learn feature representations utilizing numerous convolution kernels and deploying the activation function.

The kernel size in the proposed system is determined utilizing the linear regression model. The LR approach provides the combination of kernels for the input points utilizing scalar-valued estimator as,

$$\delta_{lr(k)} = \psi\left(\sum_{k} \delta_k\left(\nabla_{sf(n)}, \nabla_{sf}\right)\gamma_k\right) \quad (25)$$

Here, the linear combination of kernels produced utilizing the scalar-valued function $(\psi)$ is signified as $\delta_{lr(k)}$, $\delta_k$ depicts the scaled kernel at given input points $(\nabla_{sf(n)}, \nabla_{sf})$, and $\gamma_k$ is the scaling factor.

The feature value obtained from the convolution layer is signified as,

$$\nabla_{con(n,k)} = \nabla_{sf(n)} * \theta_{\delta_{lr(k)}} + \varepsilon_k \quad (26)$$

Where, the convolution layer's output is signified as $\nabla_{con(n,k)}$, the weight vector of the $k^{th}$ kernel is depicted as $\theta_{\delta_{lr(k)}}$, and $\varepsilon_k$ signifies the bias term. Next, the activation function detects non-linear features by adding non-linearities to the output. It can be given as,

$$\nabla_{non-lin(n,k)} = \begin{cases} g.\left(\nabla_{con(n,k)}\right)^g & if\left(\nabla_{con(n,k)} < 0\right) \\ g * \exp\left(\nabla_{con(n,k)} - 1\right) & if\left(\nabla_{con(n,k)} > 0\right) \end{cases} \quad (27)$$

Here, $\nabla_{non-lin(n,k)}$ are the detected non-linear features, and $g$ is the learnable parameter. Kernel size variation and SLT activation mechanisms have some advantages, such as reducing the model's complexity to explore each data point and making the network experience a faster learning process utilizing the activation function's calculations.

Next, the input's dimensionality is reduced by the pooling layer with the help of the max pooling technique. The pooling layer's feature maps are obtained as,

$$\nabla_{poo(n,k)} = \nu_{\max}\left(0, \nabla_{non-lin(n,k)}\right) \quad (28)$$

Here, the pooling layer's output is signified as $\nabla_{poo(n,k)}$, and the max pooling operation is depicted as $\nu_{\max}$.The final feature maps are flattened and fed to the fully connected layer after some executions of convolution and pooling operations to produce class scores from the activations for classification.

To produce the total number of output nodes, the softmax function is utilized in the output layer. The softmax function is derived as,

$$\xi_{(DR,NDR)} = \frac{\exp\left(\nabla_{flt(n)}\right)}{\sum_n \exp\left(\nabla_{flt(n)}\right)} \quad (29)$$

Here, $\nabla_{flt(n)}$ indicates the flattened one-dimensional feature vector, $\xi_{(DR,NDR)}$ signifies the softmax output that classifies the input images into two categories, namely patents with DR $\xi_{(DR)}$ and without DR $\xi_{(DR)}$. The classification process utilizing LRKSA-CNN is explained in Algorithm 2.

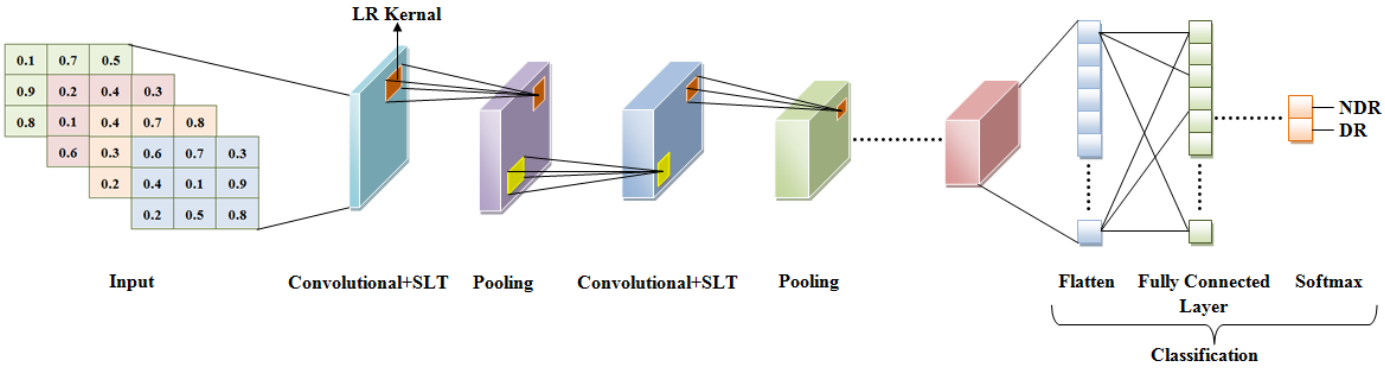


Fig. 2. Architecture of proposed LRKSA-CNN.

Algorithm .2. Classification using LRKSA-CNN

**Input:** Selected features $\nabla_{sf(n)}$

**Output:** Classified results $\xi_{(DR,NDR)}$

**Begin**

**Initialize** input $\nabla_{sf(n)}$, number of layers, model parameters $\theta_{\delta lr(k)}$, $\varepsilon_k$

**For** each layer **do**

**Generate** linear combination of kernels $\theta_{\delta lr(k)}$

**For** each kernel size **do** // convolution layer

**Compute** feature maps $\left(\nabla_{con(n,k)}\right)$

**Detect** non-linearities $\left(\nabla_{non-lin(n,k)}\right)$

**If** $\left(\nabla_{con(n,k)} < 0\right)$

$$\nabla_{non-lin(n,k)} = g.\left(\nabla_{con(n,k)}\right)^g$$

**Else**

$$\nabla_{non-lin(n,k)} = g * \exp\left(\nabla_{con(n,k)} - 1\right)$$

**End if**

**End for**

**Compute** pooled feature map $\nabla_{poo(n,k)}$

**End for**

**Generate** one dimensional feature vector $\nabla_{flt(n)}$

**Return** classified results $\xi_{(DR,NDR)}$

**End**

*F. Stages Identification*

From the classified results, the images with DR $\left(\xi_{(DR)}\right)$ are utilized for the formulation of grading to differentiate its severity into 5 stages, including severe NPDR, moderate NPDR, Mild NPDR, proliferative DR, and referable DR. Here, the KM-ANFIS is utilized for stages' identification. The ANFIS is selected since it has the advantage of having both numerical and linguistic knowledge. However, the membership function utilized in the traditional ANFIS causes the loss of interpretability in larger inputs. Thus, the Krusinka membership function is used here.

The features extracted from the retinal layers and visual network areas of DR-diagnosed images $\xi_{(DR)}$ were merged and used by the KM-ANFIS technique for stage identification. The KM-ANFIS structural design utilizes these features to form fuzzy if-then rules for grading.

Primarily, each node in the initial layer passes the input $\phi_{inp} = \left\{\xi_{(DR)}, \nabla_{fea \in R_{segO(n)}}, \nabla_{fea \in R_{segM(n)}}\right\}$ to the subsequent layers. For generating membership grades to the input, the nodes in layer 2 have a membership function. The Krusinka Membership function utilized in the proposed system is calculated as,

$$KMF\left(\phi_{inp}\right) = \frac{1}{2} + \frac{1}{\pi} arc\tan\left(\frac{\phi_{inp} - u}{v}\right) \quad (30)$$

Here, $KMF\left(\phi_{inp}\right)$ is the membership function, and $(u, v)$ are the parameters set to change the membership function's shape. The KM membership function better interprets all the inputs in a fuzzy set by its ability to capture the interaction between variables and provide a reasonably smooth transition.

In Layer 3**,** each rule's firing strength $\left(fs_{(i)}\right)$ is computed utilizing fixed nodes through multiplication. Every single node output signifies the rule's firing strength; thus, the fuzzy AND operation is performed by the nodes.

$$fs_{(i)} = KMF.\nabla_{fea \in R_{segO(n)}} \times KMF.\nabla_{fea \in R_{segM(n)}} \quad (31)$$

Rule 1:If $\nabla_{fea \in R_{segO(n)}}$ is $\varsigma_p$ and $\nabla_{fea \in R_{segM(n)}}$ is $\xi_a$, then

$$\Delta_i = h_i \nabla_{fea \in R_{segO(n)}} + f_i \nabla_{fea \in R_{segM(n)}} + \sigma_i \quad (32)$$

Rule 2:If $\nabla_{fea \in R_{segO(n)}}$ is $\varsigma_a$ and $\nabla_{fea \in R_{segM(n)}}$ is $\xi_p$, then

$$\Delta_{i+1} = h_{i+1} \nabla_{fea \in R_{segO(n)}} + f_{i+1} \nabla_{fea \in R_{segM(n)}} + \sigma_{i+1} \quad (33)$$

Here, $\varsigma_p$, $\xi_a$, $\varsigma_a$ and $\xi_p$ indicate the fuzzy sets, $h_i$, $f_i$, $\sigma_i$, $h_{i+1}$, $f_{i+1}$ and $\sigma_{i+1}$ values are the parameter set, and $\Delta$ is a first-order polynomial and signifies the fuzzy inference system's outputs.

Layer 4 computes the ratio of each rule's firing strength to the sum of all rules' firing strengths. It can be given as,

$$\overline{fs_i} = \frac{fs_i}{fs_1 + fs_2}, \quad i = 1, 2 \quad (34)$$

There is only one node in the final output layer, which computes the sum of every output from the nodes of layer 5 for producing the overall KM-ANFIS output.

$$O_{0to4} = \frac{\sum_{i=1}^{n} \overline{fs_i} \, \Delta_i}{\sum_{i=1}^{n} fs_i} \quad (35)$$

Where, $O_{0to4}$ is the overall output of the KM-ANFIS. By utilizing this, KM-ANFIS grades the DR severity into five stages. This grading scheme provides a more precise interpretation of disease stages for accurately evaluating the DR's effects in advance.

## IV. Results and Discussion

Here, the proposed DR detection approach's effectiveness is assessed by analogizing its results with prevailing techniques. In the working platform of PYTHON, the proposed technique is deployed and trained by utilizing the OCT and fMRI images gathered from publicly available sources. Fig. 3 and Fig. 4 display the sample outcomes obtained for the input images.

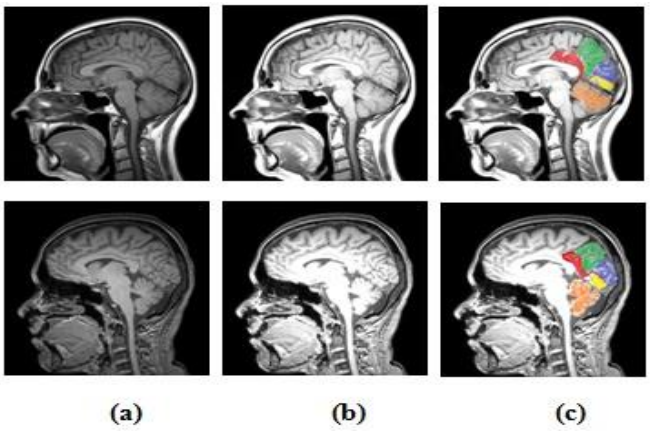


Fig. 3. (a) Input OCT images, (b) contrast-enhanced images using CLAHE, and (c) segmented regions using the ICSW-WS.

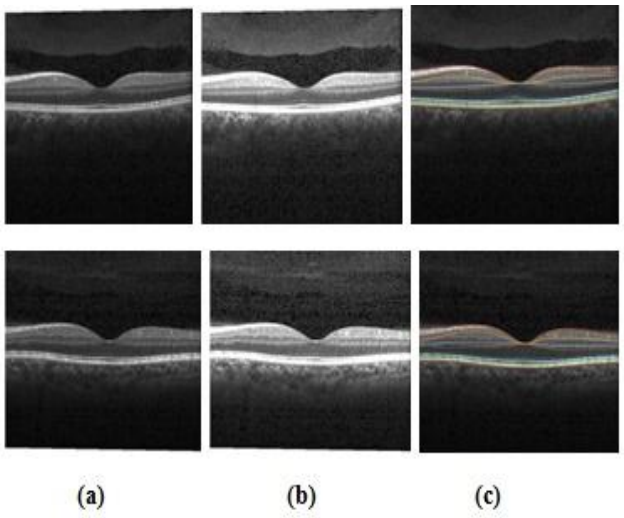


Fig. 4. (a) Input MRI images, (b) contrast-enhanced images using CLAHE, and (c) segmented regions using the ICSW-WS.

### A. Performance Analysis

This section concentrates on analyzing the outcomes of different phases, namely KM-ANFIS-based stages identification, LRKSA-CNN-based classification, ICSW-based segmentation, and MM-GAO-based feature selection for quantitatively evaluating the proposed system. The performance of LRKSA-CNN is analyzed below:

TABLE I. Performance Measure of Classification Accuracy

| Methods | Accuracy (%) |
|---|---|
| Proposed LRKSA-CNN | 97.99 |
| CNN | 92.34 |
| DNN | 93.26 |
| ANN | 90.84 |
| RNN | 88.03 |

The classification accuracy of the proposed LRKSA-CNN and traditional CNN, DNN, ANN, and Recurrent Neural Network (RNN) techniques is displayed in Table I. This table reveals that the proposed technique's classification accuracy enhanced by 4.65% than the prevailing CNN. Thus, the use of LR-based kernels *includes large information with different dimensions and* efficiently increases the classification accuracy.

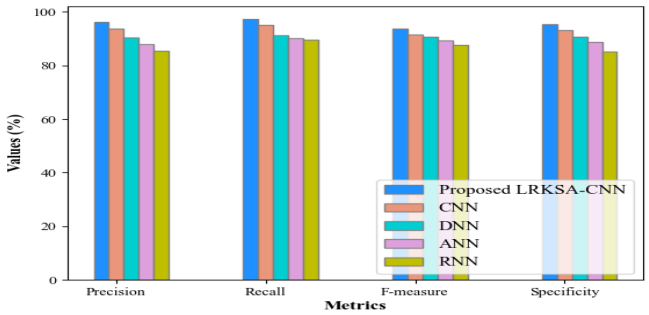


Fig. 5. Performance Analysis of LRKSA-CNN.

The proposed and conventional classification techniques' performance regardingprecision, F-measure, recall, and specificity is displayed in Fig. 5. The comparison shows that the proposed system outperforms the prevailing approaches in all metrics like precision (96.15%), recall (97.28%), F-measure (93.81%), and specificity (95.27%). This analysis reveals that by capturing larger patterns and accelerating its learning rate, the performance of the proposed model for DR classification was greatly improved with the inclusion of an LR-centric kernel and SA function.

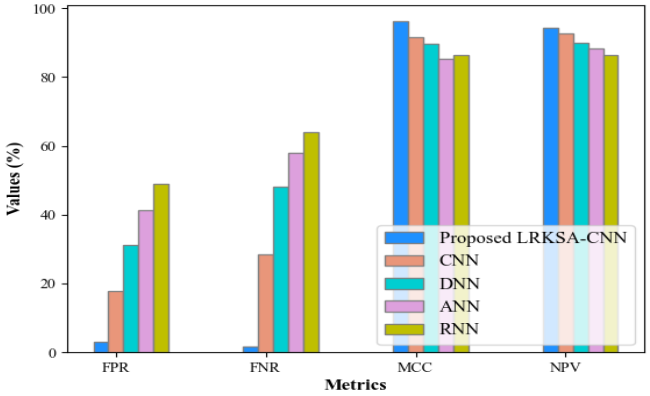


Fig. 6. Comparision of the proposed system with other classification methods.

The proposed LR-KSA technique's performance is analogized with the prevailing techniques regarding False Negative Rate (FNR), False Positive Rate (FPR), Negative Predictive Value (NPV), and Mathews Correlation Coefficient (MCC) in Fig. 6. Attaining lower values for FNR and FPR and higher values for MCC and NPV signifies better performance of the model. By the way, the proposed technique proffers superior performance regarding FNR (3.01%), FPR (1.63%), MCC (96.17%), and NPV (94.36%) analogized to the prevailingtechniques with the use of the LRKSA technique.

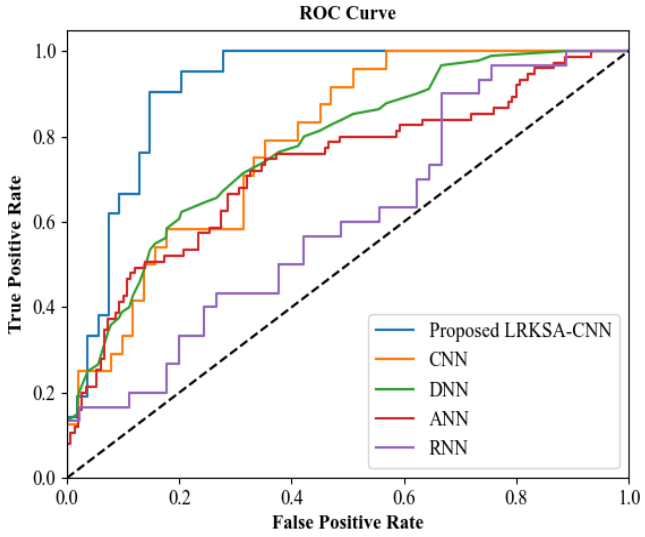


Fig. 7. ROC curve analysis.

The Receive Operative Characteristics (ROC) curve for the proposed and conventional techniques is displayed in Fig. 7. The ROC curve is for providing unbiased outcomes plotted between the true positive rate and the true negative rate. The ROC curve in Fig. 7 displays that when compared to prevailing techniques, the proposed system more accurately differentiated all classes with higher accuracy values.

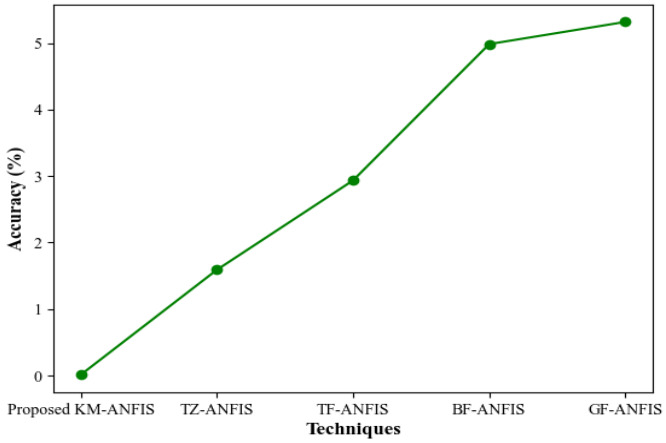


Fig. 8. Accuracy of stages identification.

The accuracy achieved by the proposed KM-ANFIS and prevailing Trapezoidal-based ANFIS (TZ-ANFIS), Triangular Function-based ANFIS (TF-ANFIS), Gaussian Function-based ANFIS (GF-ANFIS), and Bell-shaped Function-based ANFIS (BF-ANFIS) techniques are exhibited in Fig. 8. Here, the proposed technique provides higher accuracy than the prevailing techniques. The proposed system's accuracy is improved by 2.61% than the existing methods. Hence, the analysis concludes that the KM function has the efficiency to better interpret all the inputs and precisely differentiate DR stages.

TABLE II. PERFORMANCE COMPARISON OF SEGMENTATION RESULTS BASED ON VOI

| Methods | VOI |
|---|---|
| Proposed ICSW-WS | 0.0135 |
| WS | 0.0185 |
| RG | 0.0214 |
| AC | 0.0255 |
| RSM | 0.0264 |

The Variation Of Index (VOI) attained by the proposed ICSW-WS and prevailing WS, Region Growing (RG), Active Contour (AC), and Region Split and Merge (RSM) techniques are analogized in Table II. It displays that the proposed technique's VOI is much lesser by 0.005, 0.079, 0.012, and 0.013 than the prevailing WS, RG, AC, and RSm techniques. Hence, the analysis clearly defines that ICSW-centric marker identification resulted in the accurate segmentation of meaningful regions.

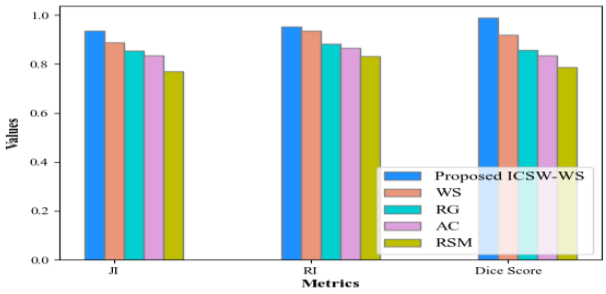


Fig. 9. Comparision of segmentation methods.

The proposed and prevailing segmentation techniques' Jaccard Index (JI), Rand Index (RI), and Dice Score (DS) are examined in Fig. 9. While comparing with prevailing techniques, the proposed technique's JI, RI, and DS are enhanced by 1.69%, 4.57%, and 6.83% than the prevailing WS technique.This indicates that the proposed ICSW-WS technique's performance was greatly influenced by the computation of ICSW weights forsegmenting small unique regions more accurately than the prevailing techniques.

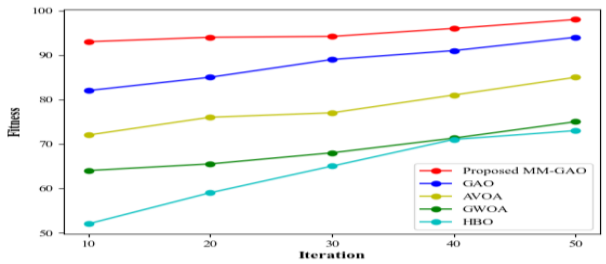


Fig. 10. Fitness vs. iteration.

The fitness values of MM-GAO and prevailing GAO, African Vultures Optimization Algorithm (AVOA), Gray Wolf Optimization Algorithm (GWOA), and Honey Badger Optimization Algorithm (HBO) techniques for 10,20,30,40, and 50 iterations are exhibited in Fig. 10. For a maximum of 50 iterations, the fitness attained by the proposed system is 98, while the prevailing techniques attained less than the proposed technique. Thus, the proposed technique is made to attain superior fitness in the given time than the prevailing techniques by the MM-centric probability calculation.

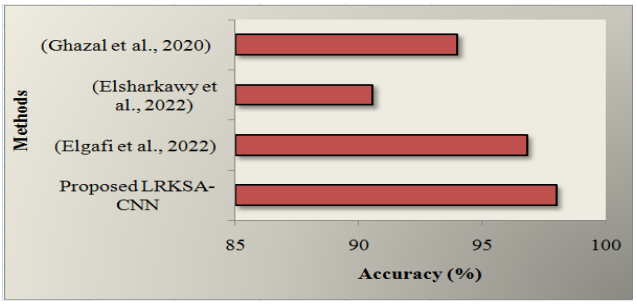


Fig. 11. Comparative analysis.

Fig. 11 analogizes the proposed LRKSA-CNN technique with the prevailing systems recommended by [17], [23], and [25] in Section II. Analyzing Fig. 11 shows that the proposed technique achieves superior performance than the prevailing techniques. Even though the prevailing techniques attained superior accuracy, they didn't concentrate on detecting DR centered on the pathophysiological changes of visual network areas.This displays the proposed system's superiority over the baseline works.

## V. CONCLUSION

An effective DR detection model based on LRKSA-CNN using multimodal images is proposed in this work. The proposed system's major goal is early DR diagnosis by examining both invisible pathologies inside the retina and microstructural changes in the visual pathway. In addition, the proposed system concentrates on classifying various phases of DR. The proposed LRKSA-CNN system is trained and evaluated utilizing MRI and OCT images. The performance analysis analogizes the proposed LRKSA-CNN and KM-ANFIS techniques with the prevailing techniques. The outcomes exhibited that the detection accuracy of LRKSA-CNN enhanced to 97.99% and KM-ANFIS to 97.46%.The overall analysis of outcomes exposed that for detecting DR and classifying all stages of DR, the proposed technique performs superior compared to the prevailing techniques. The proposed model's potential will be analyzed in the future by merging other imaging modalities. Moreover, for improving the early DR diagnosis, the blood flow changes of retinal blood vessels will be considered.

## DECLARATIONS

Funding: The authors declare that no funds, grants, or other supports were received during the preparation of this manuscript.

Competing interests: The authors have no relevant interests to disclose.

Open access : The authors declare that no funding provided for Open Access.

Author Contributions: All authors are agreed to publish the manuscript.

Availability of data and material: Not applicable.

## REFERENCES


[1] S. K. R. Meruva, V. G. S. Tulasi, N. Vinnakota, & V. Bhavana, "Risk Level Prediction of Diabetic Retinopathy based on Retinal Images using Deep Learning Algorithm", *Application 4th International Conference on Innovative Data Communication Technology and Application*, vol. *215*, pp. 722–730, 2022, https://doi.org/10.1016/j.procs.2022.12.074.

[2] N. Gundluru, D.S. Rajput, K. Lakshmanna, R. Kaluri, M. Shorfuzzaman, M. Uddin, , & M. A. Rahman Khan, "Enhancement of Detection of Diabetic Retinopathy Using Harris Hawks Optimization with Deep Learning Model", *Computational Intelligence and Neuroscience*, pp. 1–13, 2022, https://doi.org/10.1155/2022/8512469.

[3] P. Saranya, S. Prabakaran, R. Kumar, & E. Das, "Blood vessel segmentation in retinal fundus images for proliferative diabetic retinopathy screening using deep learning", *Visual Computer*, vol. 8, no. 3, pp. 977–992, 2022, https://doi.org/10.1007/s00371-021-02062-0

[4] S. Subramanian, S. Mishra, S. Patil, K. Shaw, & E. Aghajari, "Machine Learning Styles for Diabetic Retinopathy Detection: A Review and Bibliometric Analysis", *Big Data and Cognitive Computing*, vol. 6, no. 4, pp. 1–31, 2022, https://doi.org/10.3390/bdcc6040154.

[5] J. Jaskari, J. Sahlsten, T. Damoulas, J. Knoblauch, S. Sarkka, L. Karkkainen, K. Hietala, & K. K. Kaski, "Uncertainty-Aware Deep Learning Methods for Robust Diabetic Retinopathy Classification", *IEEE Access*, vol. 10, pp. 76669–76681, 2022, https://doi.org/10.1109/ACCESS.2022.3192024.

[6] H. A. H. Mahmoud, "Diabetic Retinopathy Progression Prediction Using a Deep Learning Model", *Aximos*, vol. 11, pp. 1–17, 2022.

[7] T. M. Usman, Y. K. Saheed, D. Ignace, & A. Nsang, "Diabetic Retinopathy Detection Using Principal Component Analysis Multi-Label Feature Extraction And Classification", *International Journal of Cognitive Computing in Engineering*, vol. 4, pp. 78–88, 2023, https://doi.org/10.1016/j.ijcce.2023.02.002.

[8] C. Y. Tsai, C. T. Chen, G. A. Chen, C. F. Yeh, C. T. Kuo, Y. C. Hsiao, H. Y. Hu, I. L. Tsai, C. H. Wang, J. R. Chen, S. C. Huang, T. C. Lu, & L. C. Woung, "Necessity of Predict Diabetic Retinopathy", *International Journal of Environmental Research and Public Health*, vol. 19, no. 3, pp. 1–12, 2022, https://doi.org/10.3390/ijerph19031204.

[9] I. Hossain, S. Puppala, & S. Talukder, "Collaborative Differentially Private Federated Learning Framework for the Prediction of Diabetic Retinopathy", *IEEE 2nd International Conference on AI in Cybersecurity*, *ICAIC*, pp. 1–6, 2023, https://doi.org/10.1109/ICAIC57335.2023.10044122.

[10] M. Tariq, V. Palade, Y. L. Ma, & A. Altahhan, "Diabetic Retinopathy Detection Using Transfer and Reinforcement Learning with Effective Image Preprocessing and Data Augmentation Techniques", *Intelligent Systems Reference Library*, vol. 236, pp. 1-30, 2023, https://doi.org/10.1007/978-3-031-22371-6_3.

[11] G. Alwakid, W. Gouda, & M. Humayun, "Deep Learning-Based Prediction of Diabetic Retinopathy Using CLAHE and ESRGAN for Enhancement". *Healthcare*, vol. 11, no. 6, pp. 1–17, 2023, https://doi.org/10.3390/healthcare11060863.

[12] B. Dong, X. Wang, X. Qiang, F. Du, L. Gao, Q. Wu, G. Cao, & C. Dai. "A Multi-Branch Convolutional Neural Network for Screening and Staging of Diabetic Retinopathy Based on Wide-Field Optical Coherence Tomography Angiography", *Irbm*, *43*(6), pp. 614–620, 2022. https://doi.org/10.1016/j.irbm.2022.04.004

[13] K. Gunasekaran, R. Pitchai, G. K. Chaitanya, D. Selvaraj, S. Annie Sheryl, H. S. Almoallim, S. A. Alharbi, S. S. Raghavan, & B. G. Tesemma, "A Deep Learning Framework for Earlier Prediction of Diabetic Retinopathy from Fundus Photographs", *BioMed Research International*, pp. 1-15, 2022, https://doi.org/10.1155/2022/3163496.

[14] Y. Bhawarkar, K. Bhure, V. Chaudhary, & B. Alte, "Diabetic Retinopathy Detection From Fundus Images Using Multi-Tasking Model With EfficientNet B5", *ITM Web of Conferences*, vol. 44, pp. 1-6, 2022, https://doi.org/10.1051/itmconf/20224403027.

[15] P. Zang, T. T. Hormel, T. S. Hwang, S. T. Bailey, D. Huang, & Y. Jia, "Deep-Learning–Aided Diagnosis of Diabetic Retinopathy, Age-Related Macular Degeneration, and Glaucoma Based on Structural and Angiographic OCT", *American Academy of Ophthalmology Science*, vol. 3, no. 1, pp. 1-9, 2023, https://doi.org/10.1016/j.xops.2022.100245.

[16] M. Sakthi Sree Devi, S. Ramkumar, S. Vinuraj Kumar, & G. Sasi, "Detection of diabetic retinopathy using OCT image", *Materials Today: Proceedings*, vol. 47, pp. 185–190, 2021, https://doi.org/10.1016/j.matpr.2021.04.070.

[17] M. Elgafi, A. Sharafeldeen, A. Elnakib, A. Elgarayhi, N. S. Alghamdi, M. Sallah, & A. El-Baz, "Detection of Diabetic Retinopathy Using Extracted 3D Features from OCT Images", *Sensors*, vol. 22, no. 20, pp. 1–13, 2022, https://doi.org/10.3390/s22207833.

[18] B. Menaouer, Z. Dermane, N. El Houda Kebir, & N. Matta, "Diabetic Retinopathy Classification Using Hybrid Deep Learning Approach", *SN Computer Science*, vol. 3, no. 5, pp. 1-16, 2022, https://doi.org/10.1007/s42979-022-01240-8.

[19] S. S. Mondal, N. Mandal, K. K. Singh, A. Singh, & I. Izonin, "EDLDR: An Ensemble Deep Learning Technique for Detection and Classification of Diabetic Retinopathy", *Diagnostics*, vol. 13, no. 1, pp. 1–14, 2023, https://doi.org/10.3390/diagnostics13010124.

[20] M. Murugappan, N. B. Prakash, R. Jeya, A. Mohanarathinam, G. R. Hemalakshmi, & M. Mahmud, "A novel few-shot classification framework for diabetic retinopathy detection and grading", *Measurement: Journal of the International Measurement Confederation*, vol. 200, pp. 1-14, 2022, https://doi.org/10.1016/j.measurement.2022.111485.

[21] M. M. Butt, D. N. F. A. Iskandar, S. E. Abdelhamid, G. Latif, & R. Alghazo, "Diabetic Retinopathy Detection from Fundus Images of the Eye Using Hybrid Deep Learning Features", *Diagnostics*, vol. 12, no. 7, 2022 https://doi.org/10.3390/diagnostics12071607.

[22] A. Erciyas, & N. Barişçi, "An Effective Method for Detecting and Classifying Diabetic Retinopathy Lesions Based on Deep Learning", *Computational and Mathematical Methods in Medicine*, pp. 1-13, 2021, https://doi.org/10.1155/2021/9928899.

[23] M. Elsharkawy, A. Sharafeldeen, A. Soliman, F. Khalifa, M. Ghazal, E. El-Daydamony, A. Atwan, H. S. Sandhu, & A. El-Baz, "A Novel Computer-Aided Diagnostic System for Early Detection of Diabetic Retinopathy Using 3D-OCT Higher-Order Spatial Appearance Model", *Diagnostics*, vol. 12, no. 2, pp. 1-14, 2022, https://doi.org/10.3390/diagnostics12020461.

[24] W. L. Alyoubi, M. F. Abulkhair, & W. M. Shalash, "Diabetic retinopathy fundus image classification and lesions localization system using deep learning", *Sensors*, vol. 21, no. 11, pp. 1–22, 2021, https://doi.org/10.3390/s21113704.

[25] M. Ghazal, S. S. Ali, A. H. Mahmoud, A. M. Shalaby, & A. El-Baz, "Accurate Detection of Non-Proliferative Diabetic Retinopathy in Optical Coherence Tomography Images Using Convolutional Neural Networks", *IEEE Access*, vol. 8, pp. 34387–34397, 2020, https://doi.org/10.1109/ACCESS.2020.2974158.

[26] S. K. Sahu, A. D. Sawarkar, A. K. Sahu, A. Anjikar, A. P. Bhopale and J. Chakole, "Analysis of Transfers Learning Techniques for Early Detection and Grading of Diabetic Retinopathy on Retinal Images," *2023 International Conference on Advanced Computing Technologies and Applications (ICACTA)*, Mumbai, India, pp. 1-6, 2023, doi: 10.1109/ICACTA58201.2023.10392325.

[27] S. Goswami, K. Ashwini and R. Dash, "Grading of Diabetic Retinopathy using iterative Attentional Feature Fusion (iAFF)," *International Conference on Computing Communication and Networking Technologies (ICCCNT)*, Delhi, India, pp. 1-5, 2023, doi: 10.1109/ICCCNT56998.2023.10307892.

[28] N. Z. Abidin and A. Ritahani Ismail, "Federated Deep Learning for Automated Detection of Diabetic Retinopathy," *IEEE 8th International Conference on Computing, Engineering and Design (ICCED)*, Sukabumi, Indonesia, pp. 1-5, 2022, doi: 10.1109/ICCED56140.2022.10010636.

[29] O. F. Gurcan, O. F. Beyca and M. Olucoglu, "Diagnosis of Diabetic Retinopathy with Transfer Learning and Metaheuristic Algorithms," *Innovations in Intelligent Systems and Applications Conference (ASYU)*, Sivas, Turkiye, pp. 1-6, 2023, doi: 10.1109/ASYU58738.2023.10296811.

[30] M. Jahiruzzaman and A. B. M. Aowlad Hossain, "Detection and classification of diabetic retinopathy using K-means clustering and fuzzy logic," *18th International Conference on Computer and Information*

*Technology (ICCIT)*, Dhaka, Bangladesh, pp. 534-538, 2015, doi: 10.1109/ICCITechn.2015.7488129.

[31] M. Ghazal, S. S. Ali, A. H. Mahmoud, A. M. Shalaby and A. El-Baz, "Accurate Detection of Non-Proliferative Diabetic Retinopathy in Optical Coherence Tomography Images Using Convolutional Neural Networks," in *IEEE Access*, vol. 8, pp. 34387-34397, 2020, doi: 10.1109/ACCESS.2020.2974158.

[32] H. Mustafa, S. F. Ali, M. Bilal and M. S. Hanif, "Multi-Stream Deep Neural Network for Diabetic Retinopathy Severity Classification Under a Boosting Framework," in *IEEE Access*, vol. 10, pp. 113172-113183, 2022, doi: 10.1109/ACCESS.2022.3217216.

[33] K. Aurangzeb, R. S. Alharthi, S. I. Haider and M. Alhussein, "Systematic Development of AI-Enabled Diagnostic Systems for Glaucoma and Diabetic Retinopathy," in *IEEE Access*, vol. 11, pp. 105069-105081, 2023, doi: 10.1109/ACCESS.2023.3317348.

[34] M. Nur-A-Alam, M. M. K. Nasir, M. Ahsan, M. A. Based, J. Haider and S. Palani, "A Faster RCNN-Based Diabetic Retinopathy Detection Method Using Fused Features From Retina Images," in *IEEE Access*, vol. 11, pp. 124331-124349, 2023, doi: 10.1109/ACCESS.2023.3330104.

[35] R. Pires, H. F. Jelinek, J. Wainer, S. Goldenstein, E. Valle and A. Rocha, "Assessing the Need for Referral in Automatic Diabetic Retinopathy Detection," *in IEEE Transactions on Biomedical Engineering*, vol. 60, no. 12, pp. 3391-3398, Dec. 2013, doi: 10.1109/TBME.2013.2278845.

[36] M. T. Islam, H. R. H. Al-Absi, E. A. Ruagh and T. Alam, "DiaNet: A Deep Learning Based Architecture to Diagnose Diabetes Using Retinal Images Only," in *IEEE Access*, vol. 9, pp. 15686-15695, 2021, doi: 10.1109/ACCESS.2021.3052477.

[37] D. Maji, A. K. Dhara, S. Maiti and G. Sarkar, "Efficient Net Enriched Model for Implementing the Grading of Diabetic Retinopathy Based on Retinal Blood Vessel Tortuosity," *IEEE 3rd Applied Signal Processing Conference (ASPCON)*, pp. 131-136, 2023, doi: 10.1109/ASPCON59071.2023.10396362.

[38] X. Wang *et al*., "UD-MIL: Uncertainty-Driven Deep Multiple Instance Learning for OCT Image Classification," in *IEEE Journal of Biomedical and Health Informatics*, vol. 24, no. 12, pp. 3431-3442, 2020, doi: 10.1109/JBHI.2020.2983730.

[39] M. M. Farag, M. Fouad and A. T. Abdel-Hamid, "Automatic Severity Classification of Diabetic Retinopathy Based on DenseNet and Convolutional Block Attention Module," in *IEEE Access*, vol. 10, pp. 38299-38308, 2022, doi: 10.1109/ACCESS.2022.3165193.

[40] T. Liu *et al*., "A Novel Diabetic Retinopathy Detection Approach Based on Deep Symmetric Convolutional Neural Network," in *IEEE Access*, vol. 9, pp. 160552-160558, 2021, doi: 10.1109/ACCESS.2021.3131630.

[41] G. T. Reddy *et al*., "Analysis of Dimensionality Reduction Techniques on Big Data," in *IEEE Access*, vol. 8, pp. 54776-54788, 2020, doi: 10.1109/ACCESS.2020.2980942.

[42] E. O. Rodrigues, A. Conci and P. Liatsis, "ELEMENT: Multi-Modal Retinal Vessel Segmentation Based on a Coupled Region Growing and Machine Learning Approach," in *IEEE Journal of Biomedical and Health Informatics*, vol. 24, no. 12, pp. 3507-3519, 2020, doi: 10.1109/JBHI.2020.2999257.

[43] S. Wang *et al*., "Localizing Microaneurysms in Fundus Images Through Singular Spectrum Analysis," in *IEEE Transactions on Biomedical Engineering*, vol. 64, no. 5, pp. 990-1002, 2017, doi: 10.1109/TBME.2016.2585344.

[44] K. Shankar, Y. Zhang, Y. Liu, L. Wu and C. H. Chen, "Hyperparameter Tuning Deep Learning for Diabetic Retinopathy Fundus Image Classification," in *IEEE Access*, vol. 8, pp. 118164-118173, 2020, doi: 10.1109/ACCESS.2020.3005152.

[45] B. Yang, T. Li, H. Xie, Y. Liao and Y. P. P. Chen, "Classification of Diabetic Retinopathy Severity Based on GCA Attention Mechanism," in *IEEE Access*, vol. 10, pp. 2729-2739, 2022, doi: 10.1109/ACCESS.2021.3139129.

[46] I. Usman and K. A. Almejalli, "Intelligent Automated Detection of Microaneurysms in Fundus Images Using Feature-Set Tuning," in *IEEE Access*, vol. 8, pp. 65187-65196, 2020, doi: 10.1109/ACCESS.2020.2985543.

[47] B. Abdillah, A. Bustamam and D. Sarwinda, "Classification of diabetic retinopathy through texture features analysis," *International Conference on Advanced Computer Science and Information Systems (ICACSIS)*, pp. 333-338, 2017, doi: 10.1109/ICACSIS.2017.8355055.

[48] M. J. J. P. van Grinsven, B. van Ginneken, C. B. Hoyng, T. Theelen and C. I. Sánchez, "Fast Convolutional Neural Network Training Using Selective Data Sampling: Application to Hemorrhage Detection in Color Fundus Images," in *IEEE Transactions on Medical Imaging*, vol. 35, no. 5, pp. 1273-1284, 2016, doi: 10.1109/TMI.2016.2526689.

[49] A. Krestanova, J. Kubicek and M. Penhaker, "Recent Techniques and Trends for Retinal Blood Vessel Extraction and Tortuosity Evaluation: A Comprehensive Review," in *IEEE Access*, vol. 8, pp. 197787-197816, 2020, doi: 10.1109/ACCESS.2020.3033027.

[50] K. Wisaeng and W. Sa-Ngiamvibool, "Exudates Detection Using Morphology Mean Shift Algorithm in Retinal Images," in *IEEE Access*, vol. 7, pp. 11946-11958, 2019, doi: 10.1109/ACCESS.2018.2890426.

[51] X. Li *et al*., "Rotation-Oriented Collaborative Self-Supervised Learning for Retinal Disease Diagnosis," in *IEEE Transactions on Medical Imaging*, vol. 40, no. 9, pp. 2284-2294, 2021, doi: 10.1109/TMI.2021.3075244.

[52] G. Gupta, S. Kulasekaran, K. Ram, N. Joshi, M. Sivaprakasam and R. Gandhi, "Computer-assisted identification of proliferative diabetic retinopathy in color retinal images," *Annual International Conference of the IEEE Engineering in Medicine and Biology Society (EMBC)*, pp. 5642-5645, 2015, doi: 10.1109/EMBC.2015.7319672.

[53] R. Kommaraju and M. S. Anbarasi, "Detection of Diabetic Retinopathy (DR) Severity from Fundus Photographs using Swin Transformer," *IEEE 8th International Conference on Recent Advances and Innovations in Engineering (ICRAIE)*, pp. 1-6, 2023, doi: 10.1109/ICRAIE59459.2023.10468500.

[54] R. Gambhir, S. Bhardwaj, A. Kumar and R. Agarwal, "Severity Classification of Diabetic Retinopathy using ShuffleNet," 2021 *International Conference on Intelligent Technologies (CONIT)*, pp. 1-5, 2021, doi: 10.1109/CONIT51480.2021.9498569

## AUTHORS' PROFILE

Rachna Kumari received Mtech Degree in computer science and engineering from Guru Jambheshwar University of Science and Technology. She is currently pursuing PhD Degree from GJU S&T hisar

Sanjeev Kumar received the Ph.D. degree in computer science and engineering from Guru Jambheshwar University of Science and Technology. He is currently working as Professor in GJU S&T hisar. He has authored more than 15 publications.

Sunila Godara received the Ph.D. degree in computer science and engineering from Guru Jambheshwar University of Science and Technology. She is currently working as Professor in GJU S&T hisar. She has authored more than 15 publications